AIMS Mathematics, 11(6): 17354–17381.
DOI: 10.3934/math.2026710
Received: 25 March 2026
Revised: 02 June 2026
Accepted: 04 June 2026
Published: 15 June 2026

https://www.aimspress.com/journal/Math

Research article

Mining blast vibration forecasting based on a deep learning machine optimized by improved dung beetle optimization

Ting Zhu[1,2] and Hui Lan[1,2,3,*]

[1] State Key Laboratory of Precision Blasting, Jianghan University, Wuhan 430056, China
[2] Hubei Province Key Laboratory of Engineering Blasting, Jianghan University, Wuhan 430056, China
[3] School of Artificial Intelligence, Jianghan University, Wuhan 430056, China

* **Correspondence:** Email: huilan@jhun.edu.cn.

Abstract: The ground vibrations resulting from mining blasting operations represent the most considerable adverse impact on local inhabitants and the surrounding environment. Precisely forecasting blasting vibrations with a constrained amount of monitoring data is a feasible strategy to manage ground vibrations. This research introduced an innovative hybrid modeling approach that leverages the maximal information coefficient (MIC), deep extreme learning machine (DELM), and improved dung beetle optimization (IDBO) to predict both the peak particle velocity (PPV) and frequency. Initially, feature selection was conducted utilizing the MIC algorithm. Following this, the variables identified by the MIC were employed as inputs to construct the DELM model. To enhance the DELM model's performance, the IDBO was implemented to optimize the DELM model's hyperparameters. The findings from the experiment show that the maximum root mean squared error (RMSE), mean squared error (MSE), and R^2 of the proposed hybrid framework are only 0.237, 0.108, and 0.975, respectively. These outcomes indicate that the hybrid MIC-IDBO-DELM model holds great potential as a predictive tool for blasting vibration prediction.

Keywords: ground vibration; blasting; machine learning; hybrid model; MIC-IDBO-DELM
Mathematics Subject Classification: 68T05, 90C59

1. Introduction

Blasting is widely recognized to generate adverse environmental impacts around mining sites, such as ground vibration [1], dust emissions [2,3], flyrock [4], and air blast overpressure [5,6].

Nevertheless, blasting remains the most cost-effective method for rock fragmentation and movement in mining operations [7]. With the continuous advancement of blasting technology, the upgrading of drilling and blasting equipment, and the increasing consumption of explosives, the negative consequences induced by blasting have become more prominent [8]. Among these detrimental effects, blasting vibration is always the primary concern, as it threatens the stability of reserved rock masses, affects nearby structures, and compromises the safety and comfort of local residents [9,10].

During rock blasting, the energy released by explosives generates a large amount of unconsumed energy, which propagates outward from blast holes in the form of seismic waves and eventually manifests as ground vibration [11,12]. The environmental problems induced by blasting vibration are typically cumulative, and have become increasingly severe with long-term mining operations. In recent years, the number of environmental disputes and lawsuits related to blasting-induced ground vibration has been rising, which has attracted extensive attention from both regulatory agencies and mining enterprises. To control the intensity of blasting vibration within a safe range, many standards and safety guidelines have been formulated [13,14]. Meanwhile, a large number of studies have been conducted to analyze and assess the potential risks posed by blasting-induced ground vibration [15,16].

Historically, the core goal of mine blasting design has been to attain satisfactory rock fragmentation [17]. As a result, the issue of ground vibration induced by blasting has long been overlooked. However, for blasting engineers, although a rational design should prioritize fragmentation performance, it is also essential to strictly control ground vibration within allowable safety limits [18]. To realize this goal, all factors that affect blasting vibration must be fully considered at the design stage. Unfortunately, this is often difficult to implement in practice, because accurate measurements of some influencing factors are either hard to obtain in field conditions or require considerable time and cost. The intensity of blasting vibration is governed by a variety of factors [19,20], which can be generally divided into two categories: uncontrollable factors and controllable factors [21]. Uncontrollable factors remain unchanged during blasting operations and are mainly determined by geological conditions and the physical properties of the rock mass to be excavated. Therefore, engineers usually adopt a basic design scheme first, and then revise it according to the actual geological and engineering conditions of the mine. In contrast, controllable factors, such as blasting parameters and explosive properties, can be flexibly adjusted to offset the adverse impacts caused by uncontrollable factors. Accurate prediction of blasting vibration is regarded as an effective management approach. Such predictions are used to judge whether the generated vibration level is acceptable and to provide practical suggestions for optimizing blasting design, so as to reduce structural damage and disturbance to nearby residents. Accordingly, the precise evaluation of ground vibration is critical to the scientific planning and safe implementation of blasting operations [22].

Initially, peak particle velocity (PPV) was the only indicator adopted to evaluate structural damage induced by blasting, acting as the primary safety control threshold. However, several cases have demonstrated that severe structural damage can still occur even when PPV values are well below the specified safety limits [23]. In response, many scholars have emphasized the importance of vibration frequency, noting that the dynamic response of structures is closely related to the frequency characteristics of blasting vibrations [24–26]. Currently, both PPV and frequency are widely accepted as core evaluation indicators in most safety standards, owing to their strong correlation with structural damage and human comfort [27–29]. Therefore, PPV and frequency are selected as the two prediction targets of blasting-induced vibrations in this study.

Adopting a scientific method for predicting blasting vibrations is critically important, as it can substantially improve prediction accuracy and reliability. Numerous scholars have conducted extensive research on blasting vibration prediction, and the corresponding prediction models can be

mainly classified into two categories: empirical models based on simplified field observations [30] and artificial intelligence-based machine learning models [31,32]. In practical applications, empirical models commonly rely only on limited parameters such as distance and maximum charge per delay to establish prediction formulas [33,34], resulting in relatively low prediction precision. To overcome the inherent limitations of empirical models, an increasing number of researchers have applied machine learning (ML) techniques to blasting vibration prediction. ML approaches exhibit strong capabilities in nonlinear mapping, making them highly suitable for capturing the complex nonlinear relationships between blasting parameters and ground vibration responses. Unlike empirical models, ML-based models can integrate comprehensive influencing factors as model inputs. For instance, N. Torres et al. and A. Das et al. developed prediction models using artificial neural networks (ANNs) with 15 and 13 input variables, respectively [35]. ANNs are recognized as one of the most effective ML methods for solving complex nonlinear problems and have been widely used in blasting vibration prediction. Nevertheless, like many other ML algorithms, ANNs are prone to overfitting during the modeling process [36,37]. In addition, ML models are data-driven, but collecting large-scale and high-quality blasting vibration datasets is time-consuming and laborious. Therefore, many existing blasting vibration prediction models are constructed using limited datasets.

The combination of machine learning methods with meta-heuristic algorithms has been proven to significantly improve the accuracy of blasting vibration prediction. In addition, the selection of appropriate influencing factors as model inputs plays a crucial role in determining the performance of machine learning models. Researchers including Zhu et al., Zeng et al., and Zhang et al. have adopted various strategies to screen input parameters for blasting vibration prediction [38]. However, the importance of input parameters has not been sufficiently valued in many existing models, and their actual effects are rarely evaluated before modeling. Feature selection is an essential step in model construction, which is used to quantify the correlation strength between input features and prediction targets. It can effectively simplify the model structure, shorten the training time, and improve prediction accuracy. By reasonably selecting key features, machine learning models can achieve higher efficiency and precision in blasting vibration prediction.

The deep extreme learning machine (DELM) is an innovative neural network model that augments the capabilities of the traditional ELM through the integration of self-encoder limit learning to initialize the input weights and biases of the hidden layer. This enhancement facilitates the efficient extraction of nonlinear data features. Moreover, the DELM overcomes the drawbacks of slow training speeds and prolonged prediction times that are typically encountered in conventional neural network models and analogous methodologies. For instance, many researchers [39–41] have proposed and implemented a hybrid DELM model for wind power generation forecasting. The model has demonstrated promising outcomes, thereby validating the effectiveness of the DELM. However, the DELM faces issues with its random input weights and biases, which are not amenable to inverse adjustment, predisposing it to local optima and significantly impacting the precision of forecasting.

The DELM's random initialization of input weights and biases makes it prone to getting trapped in local optima. The proposed IDBO algorithm, enhanced with chaotic mapping for initialization, an adaptive step size combined with a convex lens imaging strategy, and dynamic weighting with Lévy flight, demonstrates superior global search capability and a stronger ability to escape local optima. Therefore, employing IDBO to optimize the hyperparameters of the DELM directly addresses this core weakness, leading to a more stable and accurate predictor.

Many existing models do not adequately assess the importance of input parameters. The MIC algorithm, as a robust measure, excels at capturing both linear and nonlinear relationships between various blasting parameters (e.g., distance, charge weight) and the prediction targets (PPV and

frequency). This allows for the identification of key influencing factors, thereby streamlining the model architecture and improving predictive accuracy.

In this study, a novel integrated prediction framework is proposed to further improve the prediction accuracy of PPV and frequency. Specifically, the maximal information coefficient (MIC), improved dung beetle optimization (IDBO), and deep extreme learning machine (DELM) are combined to construct a hybrid model named the MIC-IDBO-DELM. The primary objective of this research is to enhance the prediction performance of blasting vibration by employing the MIC for feature selection and using IDBO to optimize the hyperparameters of the DELM.

This paper is structured as follows. Section 2 introduces the fundamental theories of the maximal information coefficient, improved dung beetle optimization, and DELM. Section 3 details the proposed hybrid prediction framework. Section 4 presents the experimental design, results, and comprehensive analysis of the proposed method. Finally, the main conclusions and future research directions are summarized in Section 5.

2. Methodology

This section briefly introduces the core methodologies adopted in the proposed hybrid framework, including the feature selection strategy, prediction model, and improved metaheuristic optimization algorithm.

2.1. Maximal information coefficient

The maximal information coefficient (MIC) was first proposed by Reshef et al. in *Science* (2011) based on mutual information theory. As a powerful correlation metric, the MIC captures the maximum normalized mutual information through optimal discrete partitioning, enabling it to quantify complex linear and nonlinear associations between variables [42]. Moreover, the MIC exhibits strong robustness and insensitivity to outliers, making it highly suitable for measuring variable correlations in practical engineering scenarios.

Let X and Y be two finite data sets, each comprising n elements. $X = \{x_i | i = 1, \cdots, n\}$and $Y = \{y_i | i = 1, \cdots, n\}$, which are denoted as a two-dimensional ordered set $D = \{(x_i, y_i) | i = 1, \cdots, n\}$. The grid of $G = \{x \times y\}$ is utilized to divide the data space. Altering the grid division results in varying mutual information values, with the maximum value being:

$$I(D, x, y) = \max I(D|G), \tag{1}$$

where $I(D|G)$ is the mutual information value of dataset D under division G.

The value from Eq (1) is normalized and the MIC can be calculated by the following equation:

$$M(D)_{x,y} = \frac{I(D, x, y)}{\log_{\min}\{x, y\}}. \tag{2}$$

$$MIC(D) = \max_{x \times y \le B(n)} \left\{ M(D)_{x,y} \right\}. \tag{3}$$

The range of MIC is $[0,1]$. The stronger the correlation between series X and Y, the higher the

MIC value.

2.2. Deep extreme learning machine (DELM)

Huang et al. first proposed the extreme learning machine (ELM), a typical single-hidden-layer feedforward neural network. Compared with traditional neural networks, the ELM effectively enhances learning efficiency and generalization performance. This improvement is realized by randomly generating or directly assigning hidden layer node weights, while only the output layer weights need to be calculated during the training process.

Nevertheless, the ELM struggles to extract effective salient features when facing high-noise or high-dimensional data. To overcome these limitations, an autoencoder (AE) can be integrated with the ELM to construct an ELM-AE hybrid model. By stacking multiple ELM-AE modules, the deep extreme learning machine (DELM) is formed, which further improves prediction accuracy and generalization ability. The detailed structure of the DELM is presented in Figure 1, which consists of an input layer, M hidden layers, and an output layer.

A representation of identical dimensions is achieved when the quantity of nodes in the ELM-AE input layer matches the count of nodes in the hidden layer. The weights of the hidden layer outputs, denoted as α, are specified as follows:

$$\alpha = H^{-1}T, \tag{4}$$

where H denotes the hidden layer output matrix and T represents the target output matrix.

A compact representation is generated when the count of nodes in the input layer surpasses that in the hidden layer. Conversely, a sparse representation is achieved. For both compressed and sparse representations, the output weight of the hidden layer, α, can be articulated as follows:

$$\alpha = (\frac{E}{C} + H^T H)^{-1} H^T X. \tag{5}$$

E is the unit matrix, X represents the input matrix, and C denotes the regularization factor. The DELM formulation inherently includes a regularization parameter C in its solution. An appropriate $C > 0$ was used to penalize large weights and improve generalization.

During the training phase, the original input data is fed into the first hidden layer to train the initial ELM-AE module, yielding its output weight matrix. The output weights of the preceding module are then used as the input features for the next ELM-AE unit. Using this layer-by-layer unsupervised training strategy, all ELM-AE layers are fully trained in turn, and the output weight matrix of the final layer is ultimately obtained.

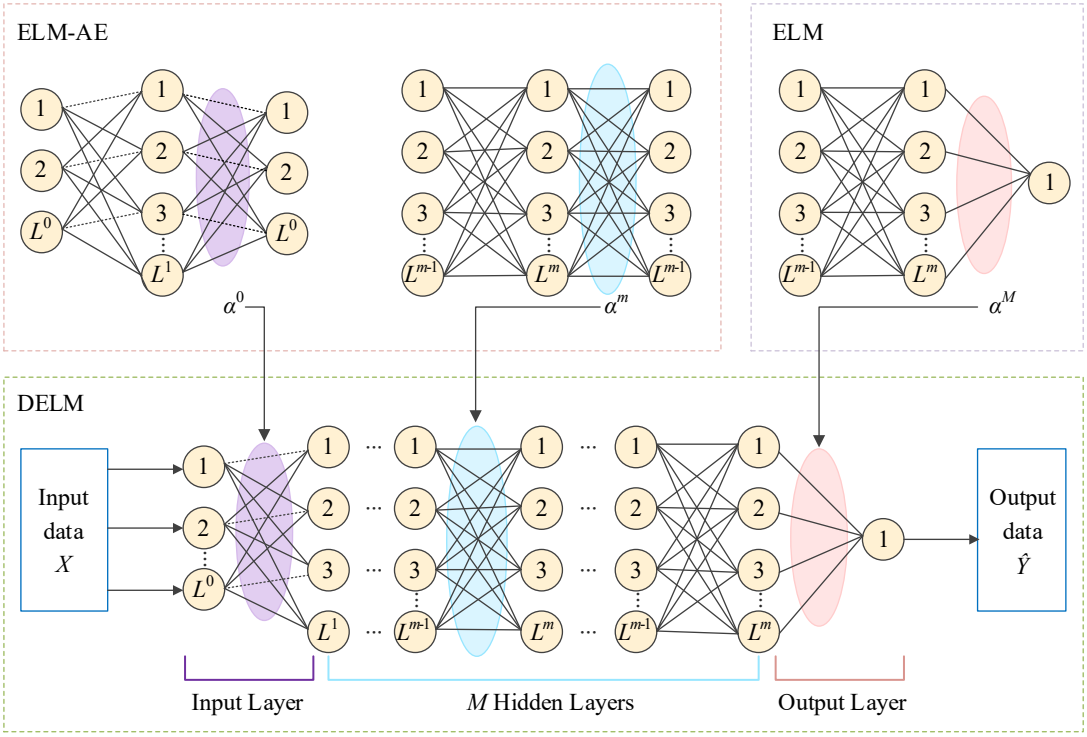

Figure 1. The structure of the DELM.

The DELM is an efficient deep model based on extreme learning machine framework, which uses autoencoder-based unsupervised pre-training to extract features layer-by-layer, rather than relying on large-scale labeled data like traditional deep neural networks. Compared with deep neural networks (DNNs) and convolutional neural networks (CNNs), the DELM has fewer parameters, faster training speed, and lower dependence on data volume, making it suitable for small-sample engineering prediction scenarios such as blasting vibration.

2.3. Dung beetle optimization (DBO)

The dung beetle optimization (DBO) algorithm, originally developed by Xue and Shen [43], is a novel swarm intelligence optimization approach. It is engineered to achieve more efficient and precise global optimal solutions by simulating the typical behavioral patterns of dung beetles, including ball rolling, dancing, breeding, foraging, and stealing behavior.

2.3.1. Ball rolling

Dung beetles utilize the sun's direction to navigate a direct route as they roll their dung balls. Equation (6) is utilized for the progressive adjustment of the dung beetle's rolling position. When faced with obstructions in its natural habitat that block its path, the beetle resorts to a dancing maneuver to ascertain a fresh direction for rolling. To replicate this behavior in a simulated environment, a stochastic value, represented by α, is integrated to ascertain the presence of obstacles during the dung ball's traversal. Upon encountering an obstacle, the beetle modifies its course by employing a tangential function. The equation for the position update of the rolling dung beetle is then represented by Eq (7).

$$x_i(t+1) = x_i(t) + \alpha k x_i(t-1) + b\left|x_i(t) - X^W\right|, \tag{6}$$

$$x_i(t+1) = x_i(t) + \tan\theta\left|x_i(t) - x_i(t-1)\right|, \tag{7}$$

where k refers to a constant value within the range $(0.0.2]$ that signifies the coefficient of deviation, α is a natural constant with a value of either 1 or –1, b represents a constant that falls within the interval $(0,1)$, X^W denotes the least-favorable location within the current group of individuals, and θ represents the turning angle that lies within the range $[0,\pi]$.When $\theta = 0,\ \pi,\ and\ \pi/2$, the position of the dung beetle engaged in ball-rolling remains stationary.

2.3.2. Breeding

In the wild, dung beetles choose a secure location for reproduction, and to emulate this instinct, the paper suggests a strategy for boundary selection to represent this zone, as outlined below in Eqs (8) and (9):

$$L_b^* = max(X^*(1 - R), L_b), \tag{8}$$

$$U_b^* = min(X^*(1 + R), U_b). \tag{9}$$

Once the dung beetle discovers the most-favorable area for reproduction, it begins the spawning process in this specific zone. Each instance of spawning for the beetle is equivalent to an iteration that refines its location. Considering the ever-changing character of the spawning zone, it ensures the exploration of the area housing the current best solution while avoiding entrapment in a local minimum. The formula for updating the position of the reproducing dung beetle is presented in Eq (10).

$$B_i(t+1) = X^* + b_1(B_i(t) - L_b^*) + b_2(B_i(t) - U_b^*). \tag{10}$$

In this formulation, X^* signifies the most advantageous position among the current population, and L_b^* and U_b^* represent the minimum and maximum limits for the position of the brood ball, respectively. $R = (1-t)/T_{max}$ denotes the nonlinear convergence coefficient, where T_{max} is the maximum number of iterations allowed, and L_b and U_b are the lower and upper boundaries for the optimization problem, respectively. $B_i(t)$ is the location of the *i*-th brood ball at the *t*-th iteration, and b_1 and b_2 are two independent random numbers.

2.3.3. Foraging

As the juvenile dung beetles mature into adulthood, they emerge from the soil to seek out sustenance. Additionally, the area designated for foraging is progressively modified with each iteration, as described by the subsequent equation:

$$Lf^b = max(X^b\left(1-R\right), L_b), \tag{11}$$

$$Uf^b = min(X^b\left(1+R\right), U_b), \tag{12}$$

$$x_i(t+1) = x_i(t) + C_1(x_i(t) - Lf^b) + C_2(x_i(t) - Uf^b). \tag{13}$$

Here, X^b represents the most-favorable position on a global scale, Lf^b and Uf^b are employed to establish the confines of the foraging territory for the young dung beetles, C_1 is a random number that follows a Gaussian distribution, and C_2 is a vector of randomness that is confined within the range from 0 to 1.

2.3.4. Stealing

Certain dung beetles opt to pilfer dung balls from their counterparts. To replicate this conduct in a model, X_b is utilized to signify the site of the disputed dung balls. The act of thievery is characterized by the position alteration of the thieving dung beetle, and this positional change is delineated by the subsequent formula:

$$x_i(t+1) = X^b + Sg(\left|x_i(t) - X^*\right|) + \left|x_i(t) - X^b\right|. \tag{14}$$

In Eq (14), g symbolizes a vector of random numbers that are normally distributed across dimension D and S represents a fixed value.

2.4. Improved dung beetle optimization (IDBO) algorithm

2.4.1. Strategy 1: Population initialization based on chaotic mapping

The DBO algorithm adopts random initialization to determine the starting positions of the dung beetle population. This strategy may result in individuals being overly concentrated, duplicated, or sparsely scattered in the solution space, thereby weakening population diversity. Given the strong ergodicity and non-repetitiveness of chaotic mapping, it can effectively enrich the diversity of the initial population and further boost the optimization efficiency of the algorithm.

While logistic and tent maps are common, they can suffer from uneven distribution in certain parameter ranges or fixed points. The composite SPM map, by combining sine and piecewise linear chaotic maps, is designed to achieve better ergodicity (more thorough coverage of the solution space) and uniformity across the entire [0,1] interval, as visually evidenced in Figure 2(a) and (b). This superior traversal property helps in generating a more diverse initial population for the IDBO, which is crucial for improving the algorithm's global exploration capability from the outset. A reference to literature discussing the properties of composite chaotic maps has been added for support.

Therefore, to overcome the limitations of random population initialization in DBO, this study combines sine mapping and a piecewise linear chaotic map to propose a new composite chaotic

mapping strategy, named the SPM. This method ensures a more uniform and ergodic distribution of the initial dung beetle population. The mathematical formulation of the SPM is given as follows:

$$Z_{n+1}=\begin{cases} mod(\dfrac{Z_n}{\eta}+\mu sin(\pi Z_n)+r,1), & 0\le Z_n<\eta, \\ mod(\dfrac{Z_n/\eta}{0.5-\eta}+\mu sin(\pi Z_n)+r,1), & \eta\le Z_n<0.5, \\ mod(\dfrac{(1-Z_n)/\eta}{0.5-\eta}+\mu sin(\pi(1-Z_n))+r,1), & 0.5\le Z_n<1-\eta, \\ mod(\dfrac{(1-Z_n)}{\eta}+\mu sin(\pi(1-Z_n))+r,1), & 1-\eta\le Z_n<1. \end{cases} \tag{15}$$

where Z_n and Z_{n+1} denote the n-th and $(n+1)$-th chaotic values. $\eta\in(0,1)$, $\mu\in(0,1)$, and r signifies a number that is randomly generated and falls within the interval from 0 to 1. $mod(\cdot)$ symbolizes the modulo operation. Figure 2 illustrates the initial distribution pattern of the SPM mapping when $\eta=0.4$ and $\mu=0.3$. It is observable in Figure 2(a) that the SPM exhibits effective traversal across the entire space, and Figure 2(b) demonstrates that the initial distribution of the SPM is highly uniform, yielding commendable outcomes.

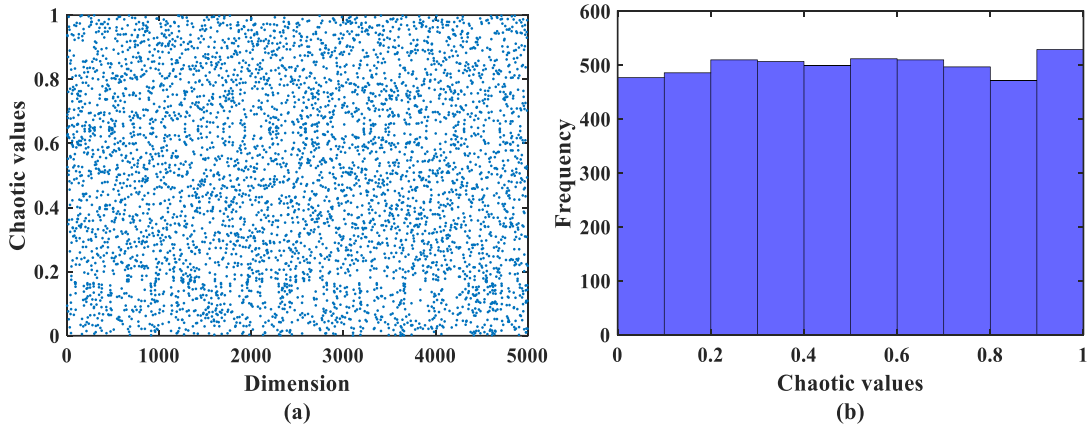

Figure 2. SPM population initialization: (a) Scatter plot; (b) Frequency distribution histogram.

2.4.2. Strategy 2: Combining an adaptive step size with the strategy of inverse imaging through a convex lens

Since the DBO algorithm relies on random searching, it lacks effective self-adjustment during the foraging process. This weakens its global exploration ability and tends to trap the algorithm in local optimal solutions. To strengthen the search performance, a dynamic selection mechanism is introduced in this study. This mechanism adaptively updates the individual position by randomly choosing between the adaptive step size strategy and the convex lens imaging strategy according to a preset probability.

In the early iteration stage, a large step size can effectively expand the foraging search range, strengthen the global exploration ability of the algorithm, help quickly find better solutions, and speed up convergence. In the later stage, a small step size is conducive to performing a refined local search. The orderly adjustment of the step size forms a directional guidance mechanism for the foraging

behavior of dung beetles, realizing the smooth transition from global exploration to local development. This strategy is mainly controlled by the linearly decreasing adaptive step adjustment factor α_0, as shown below:

$$\alpha_0 = cos[\frac{\pi}{3} \times (1 + \frac{t}{T})]. \tag{16}$$

At the same time, a convex lens imaging learning strategy is introduced to generate appropriate disturbances in the foraging dung beetle population. This mechanism effectively improves population diversity and strengthens the algorithm's ability to jump out of local optimal solutions. The mathematical expression of this strategy is given as follows:

$$P_j^* = \frac{a_j + b_j}{2} + \frac{a_j + b_j}{2k} - \frac{P_j}{k}, \tag{17}$$

where P_j represents the component of the current individual in the *j*-th dimension. a_j and b_j denote the minimum and maximum values of the *j*-th dimension, respectively. P_j^* is the convex lens inverse solution of P_j.

Ultimately, the decision on which strategy to apply for updating the target location is made based on the selection probability P_s, as expressed in Eq (18). If the stochastic value P_s is less than 0.5, a random step strategy is implemented for the position refreshment of the foraging dung beetles; on the contrary, if P_s is greater than or equal to 0.5, the position adjustments are carried out using the convex lens inverse learning strategy, as specified in Eq (19):

$$P_s = -\exp(1 - \frac{t}{T})^{10}. \tag{18}$$

$$\begin{cases} x_i(t+1) = \alpha_0 \times P_{gbest}^t + C_1 \times (P_i^t - Lf^b) + C_2 \times (P_i^t - Uf^b), & P_s < 0.5, \\ x_i(t+1) = \frac{Lf^b + Uf^b}{2} + \frac{Lf^b + Uf^b}{2k} - \frac{P_g^t best}{k}, & P_s \geq 0.5. \end{cases} \tag{19}$$

2.4.3. Strategy 3: Integrating dynamic weighting elements and Levy flight maneuvers into the formula for updating the dung beetles' positions during the act of thievery

Likewise, since X^b represents the prime food source, it attracts the thieving dung beetle. To prevent the risk of the thieving dung beetle falling into a local optimum, a dynamic weighting coefficient ω and a Levy flight mechanism have been integrated into the position update equation. This modification enhances the influence of the global optimum and the previous generation's position on the current location of the thieving dung beetle. The revised formula is presented as follows:

$$
\begin{aligned}
&x_i(t+1) = levy \times X^b + S \times g \times (\left|x_i(t) - X^*\right| + \left|x_i(t) - \omega \times X^b\right|),\\
&\omega = \frac{\exp(2\times(1-t/T_{max})) - \exp(-2\times(1-t/T_{max}))}{\exp(2\times(1-t/T_{max}) + \exp(-2\times(1-t/T_{max}))},\\
&levy = 0.01\times\mu\times r/\left|v\right|^{1/\beta},\\
&\delta_u = \left\{\frac{\tau(1+\beta)\sin(\pi\beta/2)}{2^{(\beta-1)/2}\tau[(1+\beta)/2]\beta}\right\}^{1/\beta}.
\end{aligned}
\tag{20}
$$

Here, u denotes a normally distributed variable with a mean of 0 and a standard deviation of δ_u; v and r conform to the standard normal distribution, which is utilized to produce random numbers ranging from 0 to 1; and β is a stochastic number that lies within the interval from 0 to 2.

2.4.4. Performance test of the IDBO algorithm

To verify the effectiveness of the improved dung beetle optimization (IDBO) algorithm in avoiding local optima and enhancing global search capability, comparative experiments are conducted with several representative metaheuristic approaches, including the whale optimization algorithm (WOA) [43], standard dung beetle optimization (DBO) [4], gray wolf optimization (GWO) [45], Northern Goshawk optimization (NGO) [46], and Harris hawks optimization (HHO) [47]. The parameter settings of each comparison algorithm follow the recommended values in their original literature, and the detailed configurations are summarized in Table 1.

Table 1. Parameters of the algorithms.

Algorithm	Parameter	Value
DBO	k	0.1
	b	0.3
WOA	α	[0,2]
GWO	α	[0,2]
HHO	$\jmath$	[0,2]
	β	1.5
NGO	r	[0,1]
IDBO	K	0.1
	b	0.3

The CEC2021 benchmark suite consists of a series of classical test functions, which is widely adopted to validate the performance of metaheuristic optimization algorithms. It comprises four categories of test functions: unimodal, basic, hybrid, and composite functions, allowing a comprehensive and systematic evaluation of the proposed IDBO algorithm. In this study, the CEC2021 benchmark is employed to assess the performance of IDBO, as detailed in Table 2. In particular, the unimodal function F1 is used to examine the convergence speed and exploitation ability of the algorithm. The basic functions F2 and F4 are adopted to verify its global search capability and local optimum avoidance performance. The hybrid functions F5 and F7 are applied to test its competence in solving complex optimization problems. Finally, the composite functions F8 and F10 are utilized to evaluate the stability and robustness of the algorithm in complex search spaces.

Table 2. CEC 2021 test functions.

Type	No	Function	F_{min}	Search range
Unimodal	F1	CEC01		
Basic	F2	CEC02		
	F3	CEC03		
	F4	CEC04		
Hybrid	F5	CEC05	0	[-100,100]
	F6	CEC06		
	F7	CEC07		
Composition	F8	CEC08		
	F9	CEC09		
	F10	CEC10		

All algorithmic tests are conducted under the same hardware and software environment with MATLAB 2023b to ensure fair comparison. For all algorithms, a unified population size of 30, maximum iteration of 500, and problem dimension of 20 are adopted. Each algorithm runs 30 independent trials, and its performance is evaluated using three indicators: the best value (BV), mean value (MV), and standard deviation (SD). Larger population sizes and higher iteration counts will increase computational overhead, so the combination of 30 individuals and 500 iterations is chosen as a moderate-scale setup, which can obtain stable results while controlling computing costs. The problem dimension reflects the complexity of the feature space, and high-dimensional optimization is generally more challenging. In this work, a dimension of 20 is set as a relatively rigorous test condition to verify the effectiveness of each algorithm when solving complex high-dimensional problems. Figure 3 presents the convergence curves of six algorithms over the CEC2021 test functions.

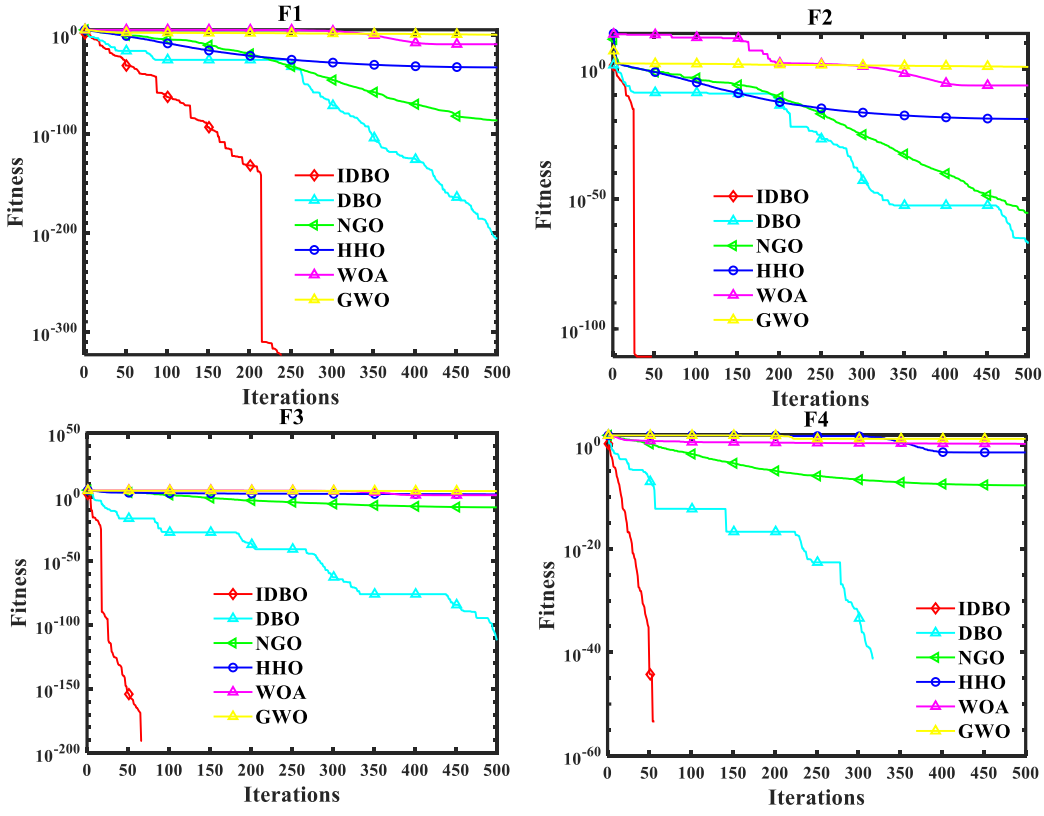

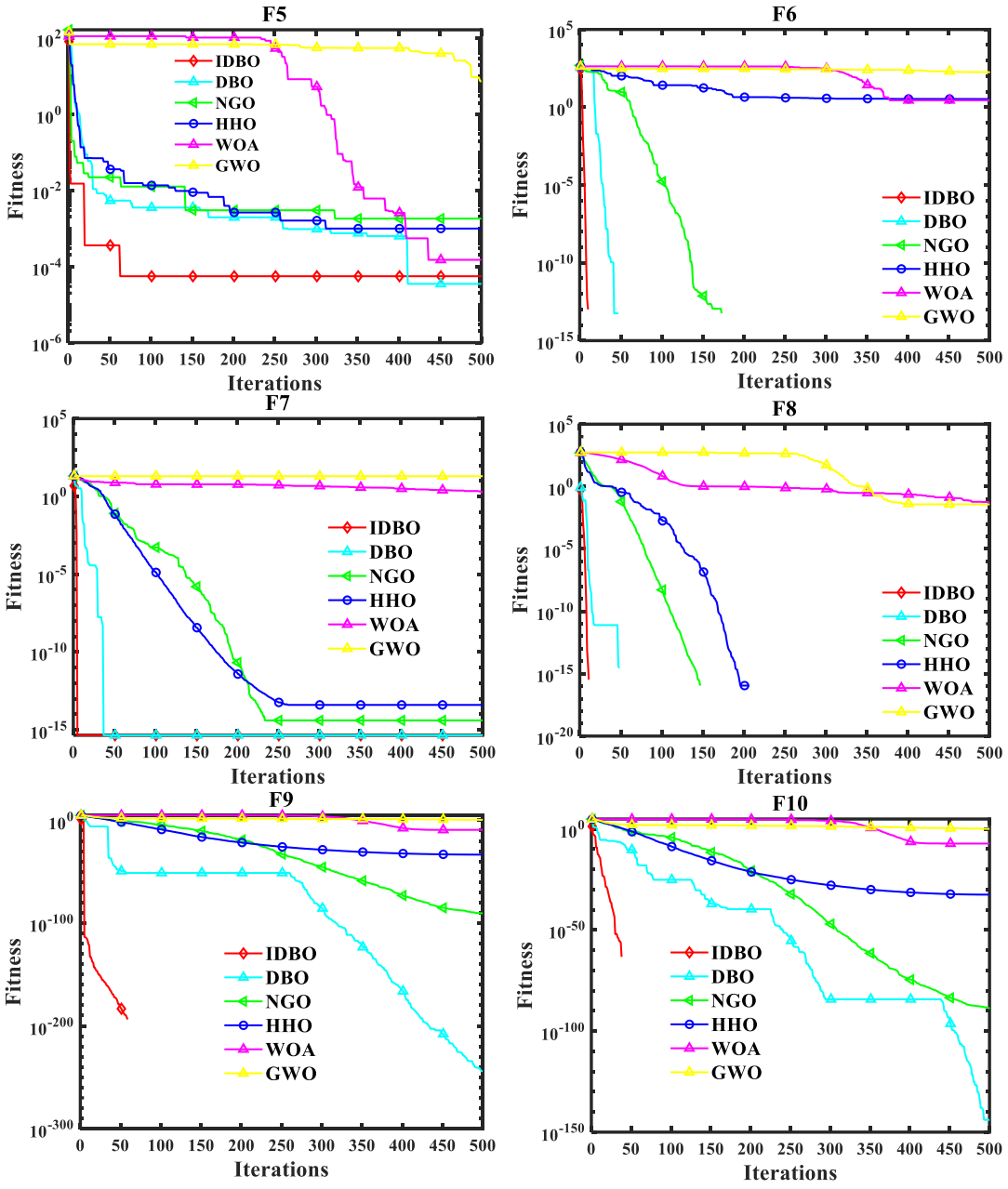

Figure 3. Convergence curves of CEC2021 test functions.

Table 3 presents the experimental results of the seven algorithms evaluated on the CEC2021 benchmark functions, with the optimal results highlighted in bold. As clearly shown in the table, the proposed IDBO algorithm exhibits superior performance over the other five comparison algorithms. Among the ten test functions, IDBO is able to converge to the theoretical optimum for all functions except F6 and F7. Although it does not attain the theoretical optimal value on the relatively complex F6 and F7 functions, IDBO still achieves a remarkable improvement over the original DBO algorithm. Furthermore, IDBO outperforms DBO consistently across all test functions, regardless of whether they are unimodal, basic, hybrid, or composite functions, suggesting that IDBO has more stable and robust optimization performance. Based on the above experimental analysis, the improved IDBO algorithm achieves higher solution accuracy and stronger optimization reliability, which fully verifies the effectiveness of the improved strategies proposed in this paper.

Table 3. Experimental results from the CEC2021 benchmark functions.

Function	Index	GWO	WOA	HHO	NGO	DBO	IDBO
F1	BV	9.43E-80	2.55E-100	3.16E-123	4.91E-105	5.59E-117	0
	SD	6.58E-67	4.66E-107	0	1.48E-29	2.20E-88	0
	MV	1.58E-67	8.42E-108	7.66E-165	5.82E-30	3.84E-90	0
F2	BV	0	0	0	1.95E-13	0	0
	SD	5.13E+02	8.72E+02	9.21E-15	3.96E+01	0	0
	MV	1.88E+02	4.43E+02	5.88E-15	2.47E+02	0	0
F3	BV	0	0	0	4.38E-26	0	0
	SD	1.76E-30	4.52E+01	0	6.26E+01	0	0
	MV	2.92E-31	1.78E+01	0	8.02E+01	0	0
F4	BV	0	0	0	0	0	0
	SD	7.28E-01	3.72E+00	0	1.38E+00	0	0
	MV	2.93E-01	1.83E+00	0	6.77E-01	0	0
F5	BV	3.91E-72	7.88E-101	1.26E-24	3.17E-19	4.33E-78	0
	SD	3.78E-16	3.43E+01	7.43E-20	3.53E+01	2.38E-80	0
	MV	6.68E-17	4.87E+00	3.72E-20	8.56E+00	6.53E-81	0
F6	BV	7.88E-08	0	4.77E-05	8.34E-02	6.12E-04	-2.2E-16
	SD	1.76E+02	1.73E+02	1.43E-04	2.58E+00	5.77E-01	7.66E-17
	MV	3.38E+01	5.75E+01	2.84E-04	2.95E+00	1.86E-01	-1.96E-14
F7	BV	9.42E-04	2.58E-08	2.66E-05	2.46E-02	4.77E-04	1.05E-16
	SD	7.88E-02	1.42E+00	7.88E-05	1.78E+00	5.88E-04	2.49E-16
	MV	6.42E-02	3.28E-01	1.82E-04	1.78E+00	2.56E-04	-1.52E-16
F8	BV	0	0	0	0	0	0
	SD	6.28E-17	0	0	0	0	0
	MV	1.26E-17	0	0	0	0	0
F9	BV	5.82E-89	5.67E-165	5.18E-34	3.68E-15	8.92E-15	0
	SD	4.52E-16	5.88E-103	3.03E-14	1.73E-15	8.62E-15	0
	MV	7.82E-16	1.05E-100	7.73E-14	4.78E-15	9.23E-15	0
F10	BV	2.78E-04	1.53E-09	6.72E-04	8.77E-03	2.72E-88	0
	SD	3.65E-02	3.77E+01	2.47E-04	3.68E+01	8.53E-79	0
	MV	9.55E-02	2.45E+01	1.28E-03	7.25E+01	3.42E-75	0

3. Datasets and description

In this investigation, the dataset encompasses variables related to explosive characteristics, geological settings, attributes of the rock, configurations of the blasts, and the monitoring data from the vibrations produced by blasting. This research utilizes a compilation of 108 instances of blasting, each with nine distinct input parameters and a pair of output parameters. Table 4 provides a statistical summary of the dataset employed in this investigation. Figure 4 presents the features' distribution as a histogram.

For each continuous variable (e.g., PPV, frequency, distance, charge, etc.), we applied the augmented Dickey-Fuller (ADF) test. Results show that all series are stationary (p-value < 0.05) after removing any obvious trends. For variables with slight trends, we applied first-order differencing.

Table 4. Description of all parameters.

Type	Indicator	Symbol	Unit	Min	Max	Mean	Std.Dev
Inputs	Maximum charge per delay	M	*kg*	160	5590	1081.1	968.7
	Total charge	T	*kg*	936	9000	4263.9	2087.1
	Distance	D	*m*	47.1	444.3	176.7	98.9
	Elevation difference	E	*M*	6	109.3	54.5	24.6
	Resistance line	R	*m*	4	7	5.4	0.8
	Pre-split penetration ratio	P	*%*	0	100	29.6	42.0
	Integrity coefficient	I	-	0.3	0.78	0.6	0.1
	Angle between resistance line and measurement station	A	°	0	180	128.0	62.7
	Velocity of detonation	V	*m/s*	2800	4200	3434.0	700.2
Outputs	PPV	PPV	*cm/s*	0.1	5.37	1.21	1.2
	Frequency	Frequency	*Hz*	14.3	51.1	34.0	10.0

The integrity coefficient I is a dimensionless parameter defined as the ratio of the average P-wave velocity in the rock mass to that in an intact rock core. In this study, it was measured using the sonic wave velocity testing method. Specifically, we drilled boreholes at each blast site, measured P-wave velocity in situ, and divided it by the laboratory-measured P-wave velocity of intact samples from the same block.

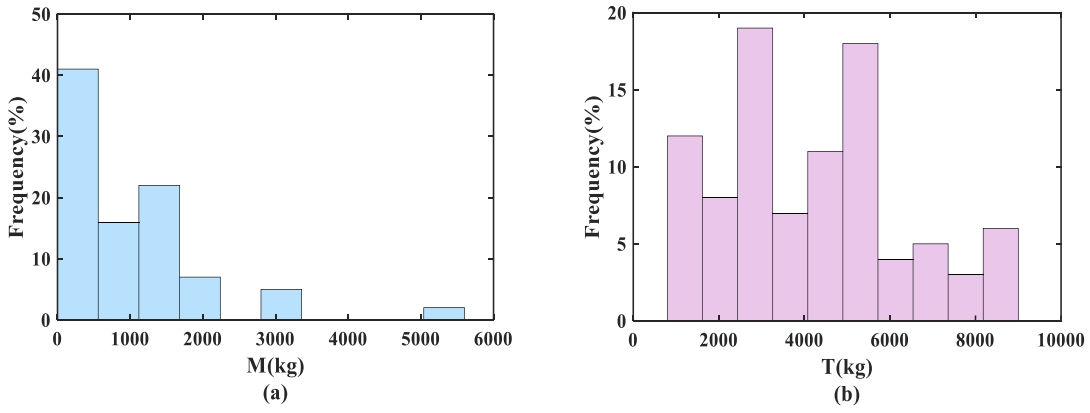

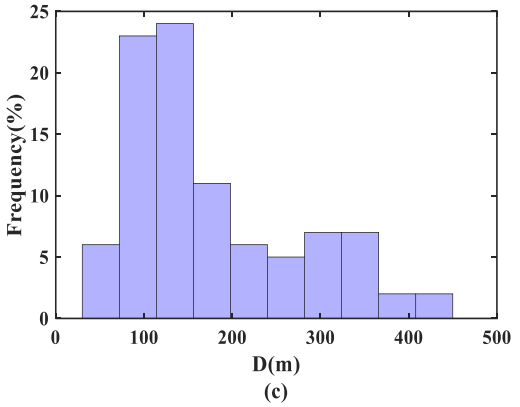
Frequency(%)
D(m)

(c)

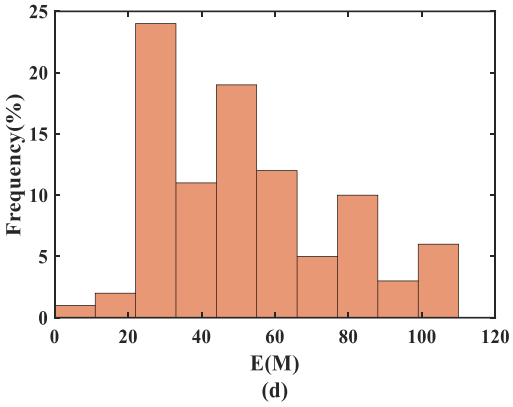
Frequency(%)
E(M)

(d)

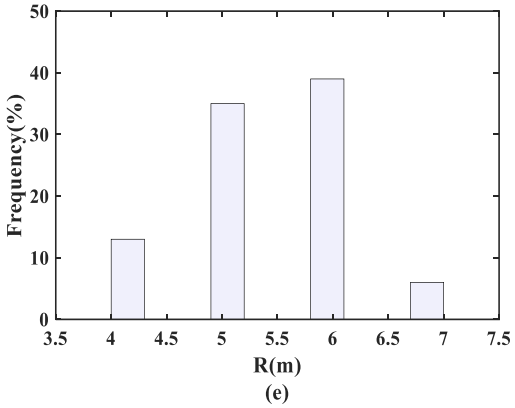
Frequency(%)
R(m)

(e)

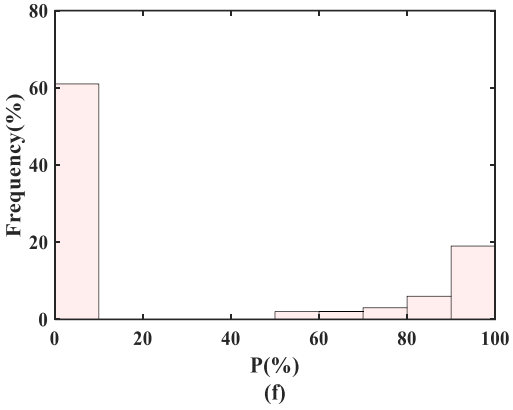
Frequency(%)
P(%)

(f)

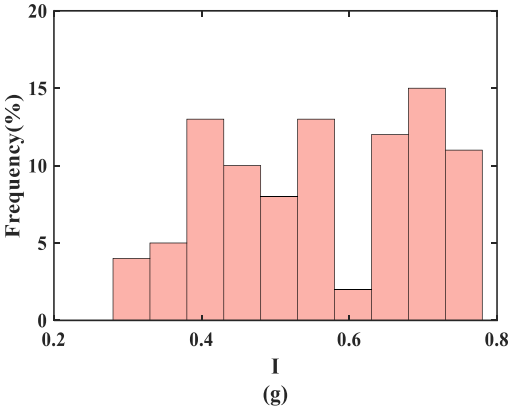
Frequency(%)
I

(g)

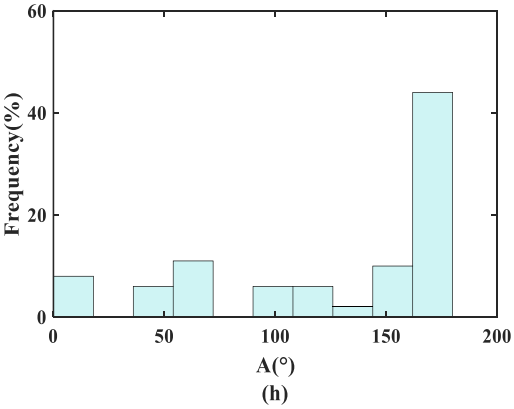
Frequency(%)
A(°)

(h)

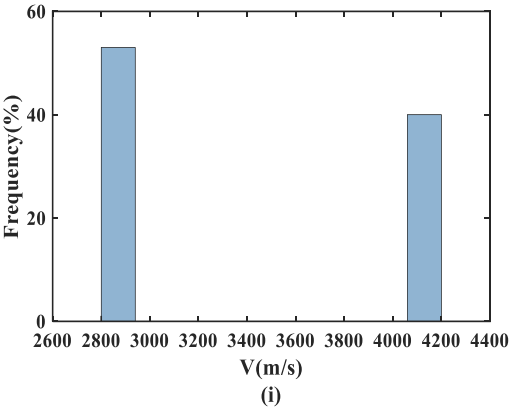
Frequency(%)
V(m/s)

(i)

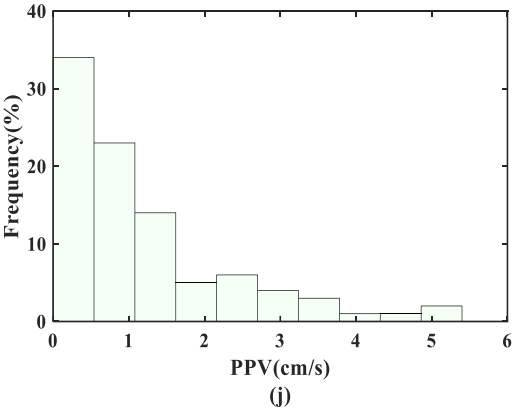
Frequency(%)
PPV(cm/s)

(j)

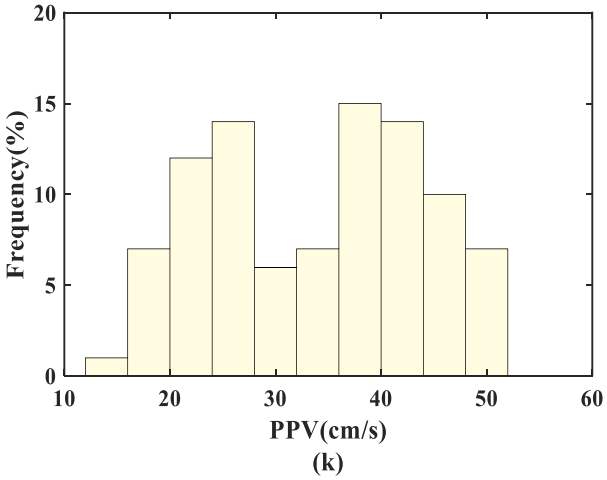

Figure 4. Histograms of the eleven features.

4. Results and discussions

4.1. Feature selection results

In this study, the maximal information coefficient (MIC) is adopted to quantify the contribution degree of each influencing factor to both PPV and frequency. Meanwhile, the MIC can effectively capture the potential indirect relationships between independent and dependent variables, thereby facilitating the identification of critical input variables for the model. The MIC analysis results corresponding to PPV and frequency are illustrated in Figures 5 and 6, respectively.

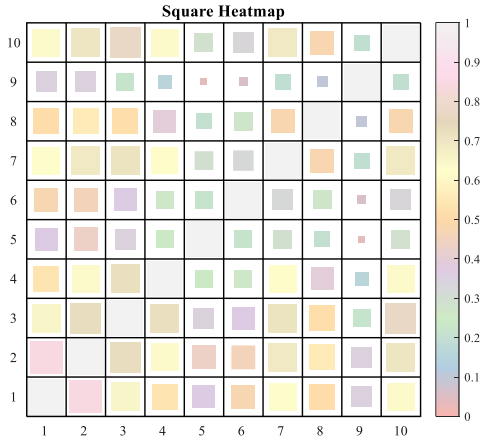

Figure 5. Thermal diagram of MIC analysis results of PPV.

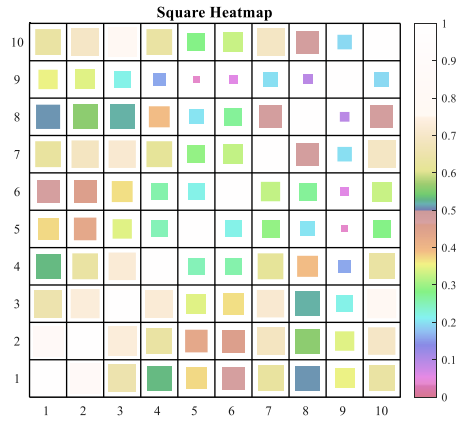

Figure 6. Thermal diagram of MIC analysis results of frequency.

Feature selection (MIC): Reducing the input dimensionality from 9 to 8/9 key features minimizes noise and irrelevant information, directly countering overfitting by simplifying the model's task. The MIC is utilized to examine the "contribution" of each factor toward the output value of the PPV and frequency.

The threshold of 0.2 was determined based on a combination of domain knowledge and statistical analysis. By examining the distribution of MIC values (as seen in Figures 5 and 6), we observed that the correlation (MIC value) for most features with the targets ranged between 0.1 and 0.5. A threshold of 0.2 effectively filters out parameters with very weak correlations (MIC < 0.2), which typically have minor or ambiguous physical influence on blast vibration in the context of our dataset.

The threshold of 0.2 was chosen based on a combination of statistical reasoning and domain knowledge. MIC values range from 0 (no relationship) to 1 (perfect relationship). A threshold of 0.2 was set to filter out features with only very weak associations, focusing on those with at least a modest correlation to the target. The distribution of MIC values in Figures 5 and 6 shows a natural gap or drop near this value.

Regarding the different treatment of the velocity of detonation (V), we now explain that the MIC analysis revealed a stronger nonlinear relationship between V and frequency (MIC > 0.2) than between V and PPV (MIC < 0.2). This aligns with the physical understanding that detonation velocity can influence the frequency spectrum of the induced vibration wave. Its exclusion from the PPV model simplifies it without significant information loss, as other factors like charge weight and distance dominate PPV prediction.

The key parameters selected by this threshold (e.g., distance D, maximum charge per delay M, integrity coefficient I, pre-split penetration ratio P) have clear physical meanings. Distance (D) is directly related to the geometric attenuation of vibration waves. The maximum charge per delay (M) is the primary source of vibration energy. The rock mass integrity coefficient (I) reflects the wave propagation and attenuation characteristics of the rock mass. The pre-split penetration ratio (P) indicates the quality of the pre-split surface, which affects the direction and isolation of blast energy. Therefore, the MIC threshold of 0.2 acts not only as a statistical filter but also aligns with the selection of parameters known to have significant physical effects in blasting engineering practice. Parameters with very low MIC values (e.g., below 0.1) were found to have an insignificant physical impact within our specific dataset and were thus removed.

Variables with a "contribution degree" greater than 0.2 are incorporated as inputs in the predictive model, as illustrated in Table 5. Following the MIC analysis, each sample comprises solely the aforementioned selected input data.

Table 5. Features after feature selection.

Type	Selected features
PPV	M、T、D、E、R、P、I、A
Frequency	M、T、D、E、R、P、I、A、V

4.2. Evaluation benchmarks

To better effectively assess the performance of the proposed algorithm, the following metrics will be utilized as the evaluation benchmarks, including root mean square error (*RMSE*), mean squared error (*MSE*) and coefficient of determination (R^2), which are defined as follows:

$$RMSE = \sqrt{\frac{1}{N}\sum_{i=1}^{N}(X_i - Y_i)^2}, \tag{21}$$

$$MSE = \frac{\sum_{i=1}^{N}(X_i - Y_i)^2}{N}, \tag{22}$$

$$R^2 = 1 - \frac{\sum_{i=1}^{N}(X_i - Y_i)^2}{\sum_{i=1}^{N}(\bar{X}_i - \bar{Y}_i)^2}. \tag{23}$$

Here, N signifies the total count of data points, i represents each individual data point, and X_i and Y_i denote the actual and forecasted values, respectively. $\bar{X}_i$ and $\bar{Y}_i$ refer to the means of actual and forecasted values, respectively.

4.3. Comparative experiments

4.3.1. Comparative experiment I

To comprehensively assess the predictive accuracy of the suggested framework, four comparative models (MIC-IDBO-DELM\IDBO-DELM\MIC-DELM\DELM) are established based on 70% of the training set and 30% of the testing set in comparative experiment I. The above four models, including the DELM and IDBO-DELM models that considered all variables as inputs and the other two that considered important variables as inputs, were utilized to establish the feasibility of the proposed hybrid framework.

The outcomes for the PPV and frequency predictions of the MIC-DELM, IDBO-DELM, and MIC-IDBO-DELM models during the testing phase are detailed in Table 6. While the PPV prediction results indicate that all models possess satisfactory precision, the hybrid MIC-IDBO-DELM model outperforms the others in terms of accuracy. The RMSEs for the DELM, MIC-DELM, IDBO-DELM,

and MIC-IDBO-DELM are 0.993, 0.814, 0.616, and 0.237, respectively, with the MIC-IDBO-DELM showing the lowest RMSE. In contrast, the DELM exhibits the highest RMSE. Corresponding observations are made regarding the MSE values, as well. In addition, R^2 values for the DELM, MIC-DELM, IDBO-DELM, and MIC-IDBO-DELM models in predicting PPV are 0.812, 0.854, 0.917, and 0.975, respectively. The highest R^2 is observed to be 0.975 from the MIC-IDBO-DELM model. The results demonstrate that the hybrid MIC-IDBO-DELM and MIC-DELM models outperform the IDBO-DELM and DELM models, respectively.

As presented in Table 6, consistent conclusions can also be drawn from the frequency prediction results. The MIC-IDBO-DELM model still achieves the best overall performance, characterized by the lowest RMSE and MSE values as well as the highest R^2 value. Specifically, the RMSE, MSE, and R^2 of MIC-IDBO-DELM are 3.273, 4.351, and 0.954, respectively, whereas those of MIC-DELM are 8.167, 12.673, and 0.823. The performance indicators in Table 6 demonstrate that integrating the MIC method for key input feature selection effectively improves the prediction performance of both the DELM and IDBO-DELM models.

Table 6. Performance metrics of different models in the test phase.

Models	PPV			Frequency		
	MSE	RMSE	R^2	MSE	RMSE	R^2
DELM	0.672	0.993	0.812	11.375	17.114	0.793
MIC-DELM	0.556	0.814	0.854	8.167	12.673	0.823
IDBO-DELM	0.412	0.616	0.917	6.381	8.356	0.881
MIC-IDBO-DELM	0.108	0.237	0.975	3.273	4.351	0.954

4.3.2. Comparative experiment II

To fully illustrate the superior prediction performance of the proposed hybrid model, four representative single models, namely, the ANN, XGBoost, AdaBoost, and Bagging, are selected for comparative validation in experiment II. Figures 7–9 and Table 7 summarize the performance metrics, including MSE, RMSE, and R^2, obtained by the proposed hybrid model and the aforementioned single models in the prediction of PPV and frequency.

Taking the MSE metric as an example, in PPV prediction, the proposed model reduces the MSE by 0.635, 0.507, 0.444, and 0.239, respectively, compared with the ANN, XGBoost, AdaBoost, and Bagging models. For the RMSE index, the corresponding reductions are 0.75, 0.63, 0.495, and 0.307.

In terms of the coefficient of determination R^2, the proposed model achieves improvements of 20.37%, 17.74%, 14.11%, and 9.03% over the four single models. Meanwhile, similar improvement trends are also obtained in frequency prediction. The above results demonstrate that the proposed hybrid framework exhibits stronger robustness and higher prediction accuracy than the individual benchmark models in PPV prediction tasks.

Table 7. Performance evaluation of the proposed model compared with four single models.

Models	PPV			Frequency		
	MSE	RMSE	R^2	MSE	RMSE	R^2
ANN	0.743	0.987	0.752	13.682	20.324	0.707
XGBoost	0.615	0.867	0.802	9.766	18.720	0.764
AdaBoost	0.552	0.732	0.841	8.775	11.446	0.808
Bagging	0.347	0.544	0.887	6.941	8.627	0.835
MIC-IDBO-DELM	0.108	0.237	0.975	3.273	4.351	0.954

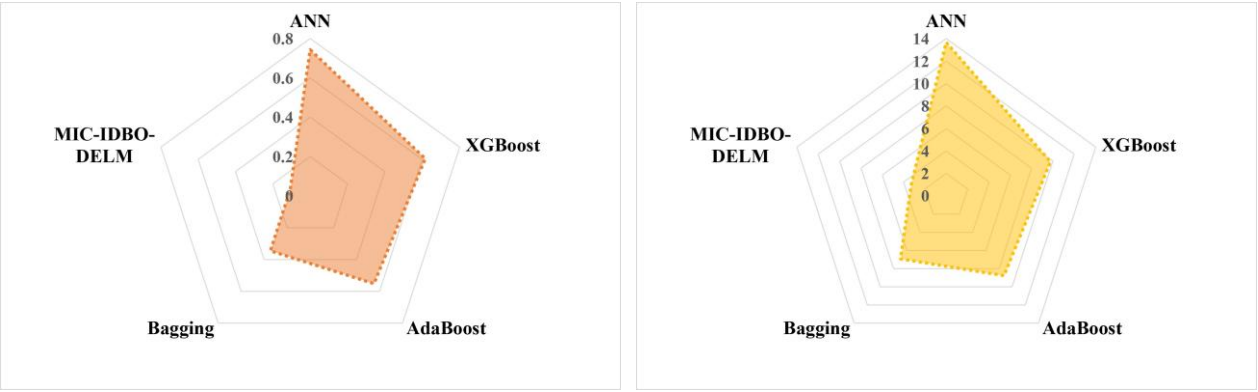

Figure 7. MSE results for PPV and frequency.

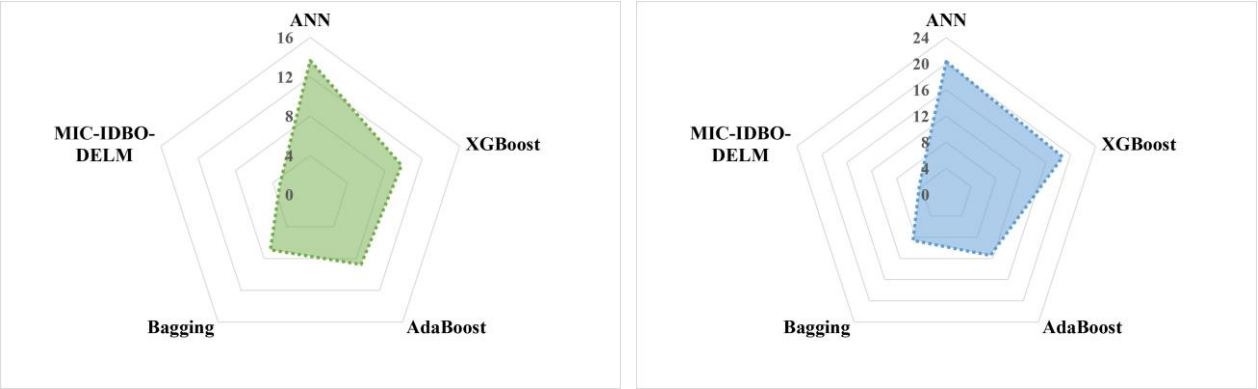

Figure 8. RMSE results for PPV and frequency.

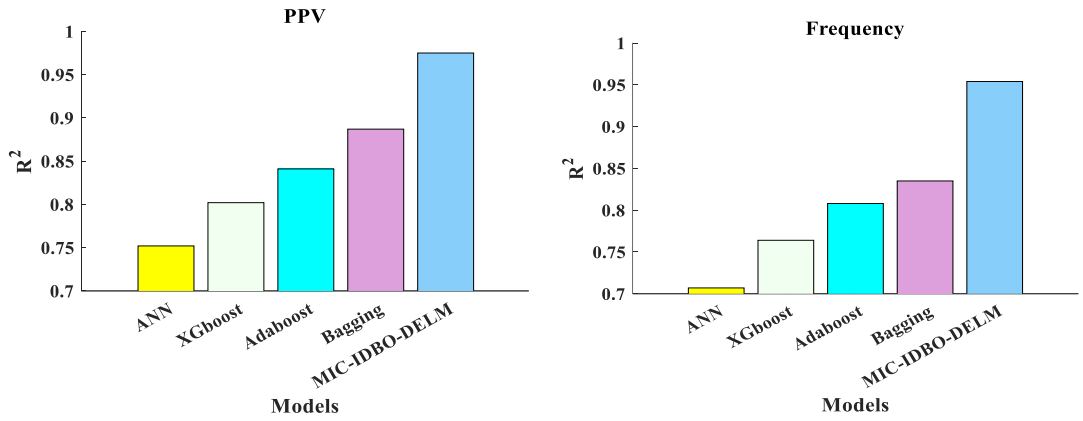

Figure 9. R^2 results for PPV and frequency.

4.3.3. Comparative experiment III

To further validate the effectiveness and advantages of the proposed method, this section compares it with representative existing approaches from recent relevant literature. The corresponding comparison results are summarized in Table 8.

As reflected by the RMSE error metric in Table 8, the proposed method achieves respective reductions of 0.216, 0.152, 1.332, 0.995, 1.524, 0.103, 1.505, and 48.63 in RMSE values compared with MRFO-SONIA, SpaSO-ELM, MARS-PSO-MLP, AutoencoderNN-SVR, HGS-ANN, HHO-RF, XGBoost, and MARs. Meanwhile, the corresponding R^2 values are enhanced by 8.36%, 6.26%, 8.09%, 9.03%, 5.44%, 3.59%, 2.36%, and 17.33%, respectively. These results clearly demonstrate that the model developed in this study surpasses the comparative models and delivers significantly improved accuracy for PPV prognosis. In summary, the prediction results obtained using the proposed hybrid model are verified to be reliable and effective.

Table 8. Comparison prediction results of different methods for PPV.

Model	RMSE	R^2
MRFO-SONIA [48]	0.453	0.896
SpaSO-ELM [49]	0.389	0.914
MARS-PSO-MLP [50]	1.569	0.902
AutoencoderNN-SVR [51]	1.232	0.887
HGS-ANN [52]	1.761	0.922
HHO-RF [53]	0.34	0.940
XGBoost [54]	1.742	0.952
MARs	48.867	0.806
This paper	0.237	0.975

5. Conclusions

Environmental concerns associated with mining blasting operations have become increasingly prominent, which makes accurate prediction of blasting vibration essential to alleviate its adverse effects. High-precision prediction models for peak particle velocity (PPV) and vibration frequency represent a practical and effective approach. In this research, a novel hybrid prediction framework is

proposed, which combines the deep extreme learning machine (DELM) with the maximal information coefficient (MIC) and improved dung beetle optimizer (IDBO) to boost the accuracy of blasting vibration prediction. In this integrated DELM model, the MIC is adopted to implement intelligent feature selection, whereas IDBO is employed to optimize the critical hyperparameters of the network.

Taking into account all nine input variables, two streamlined MIC models were constructed for the purpose of feature selection. The MIC models chose eight and nine input variables for the prediction of PPV and frequency, respectively. Subsequently, to enhance the precision of PPV and frequency forecasting, IDBO was employed to determine the hyperparameters of the DELM. The hybrid MIC-IDBO-DELM model's performance was then assessed against the DELM, MIC-DELM, and IDBO-DELM models using metrics such as MSE, RMSE, and R^2. The findings demonstrated that the hybrid MIC-IDBO-DELM model outperformed the others, achieving MSE of 0.108 $(cm/s)^2$ and 3.273 $(cm/s)^2$, RMSE of 0.237cm/s and 4.351 cm/s, and R^2 of 0.975 and 0.954 for the PPV and frequency prediction, respectively.

The MIC component of the hybrid model was capable of not only picking out crucial variables for model input but also assessing the relative significance of these selected variables. In this research, distance emerged as the paramount input variable, significantly surpassing other variables in importance. In addition, the maximum charge per delay, pre-split penetration ratio, and integrity coefficient were also identified as highly significant.

Distance (D): Confirmed as paramount due to geometric attenuation of seismic waves.

Integrity Coefficient (I): A high significance indicates that vibrations attenuate more rapidly in fractured rock masses (low I) due to increased scattering and energy dissipation at joints, whereas more intact rock (high I) transmits vibrations more efficiently and to greater distances. This physically explains its importance in the model.

Pre-split Penetration Ratio (P): A high-quality pre-split (high P) acts as a designed fracture plane, effectively reflecting and attenuating blast energy, thereby reducing the vibration behind it. The model successfully captures this engineered vibration control mechanism.

Maximum Charge Per Delay (M): The primary source of vibration energy.

The results established the viability and efficacy of the integrated MIC-IDBO-DELM model as a cost-effective, interpretable, and straightforward approach for predicting blasting vibrations. The composite model possesses significant capacity to manage intricate and multivariable nonlinear challenges, including those related to blasting vibrations. The interpretability of our hybrid model primarily stems from the MIC-based feature selection stage, which clearly ranks and selects the most influential blasting parameters (D, M, I, P). This provides actionable insights for engineers. We clarify that while the DELM itself is a complex function approximator, its internal weights are not directly human-interpretable. The model's "straightforward" nature refers to its defined pipeline (MIC→IDBO→DELM) for practical application.

The proposed MIC-IDBO-DELM framework offers a systematic design: The MIC first filters out redundant features, and then IDBO optimizes the DELM to mitigate its randomness issue. This sequential "feature selection + optimizer + core predictor" structure provides a more comprehensive solution compared to models using only a subset of these components (e.g., DELM, IDBO-DELM, MIC-DELM) and many existing hybrid models. The superior performance of this integrated approach is conclusively demonstrated by the comparative experimental results in Section 4.3.1. Note comparative experiment I, where the MIC-IDBO-DELM achieved the best metrics.

Testing the model on data from different geological settings, integrating real-time sensor data for adaptive prediction, exploring hybrid models with other deep learning architectures, and developing a user-friendly software interface for field engineers are all possible directions for future work.

Author contributions

Ting Zhu: Investigation, methodology, project administration, resources, software, supervision, validation, visualization; Hui Lan: Funding acquisition, formal analysis, writing—review and editing. All authors have read and approved the final version of the manuscript for publication.

Use of Generative-AI tools declaration

The authors declare they have not used Artificial Intelligence (AI) tools in the creation of this article.

Acknowledgments

The authors acknowledge the Natural Science Foundation of Hubei Province, China (No. 2024AFB1008), National Natural Science Foundation of China (Grant Nos. 52578584, 52478525, and U25A20355), Natural Science Foundation of Hubei Province (Grant No. 2024AFA092), National Key Research and Development Program (2021-008), Wuhan Key Research and Development Program (2024050802030155), 2024 Chutian Talent Plan-Science and Technology Innovation Team Project, Central Government-guided Local Science and Technology Development Special Project of Hubei Province (2025CSA01), Doctor Initiated Fund of State Key Laboratory of Precision Blasting [PBSKL-2025-QD-12], and Hubei Provincial Key Laboratory of Metallurgical Industry Process System Science (No. Y202401).

Conflict of interest

The authors declare no conflicts of interest.

References

1. Y. Yan, X. Hou, H. Fei, Review of predicting the blast-induced ground vibrations to reduce impacts on ambient urban communities, *J. Clean. Prod.*, **260** (2020), 121135. https://doi.org/10.1016/j.jclepro.2020.121135
2. S. Hosseini, M. Monjezi, E. Bakhtavar, Minimization of blast-induced dust emission using gene-expression programming and grasshopper optimization algorithm: a smart mining solution based on blasting plan optimization, *Clean Technol. Environ. Policy*, **24** (2022), 2313–2328. https://doi.org/10.1007/s10098-022-02327-9
3. S. Hosseini, M. Monjezi, E. Bakhtavar, A. Mousavi, Prediction of dust emission due to open pit mine blasting using a hybrid artificial neural network, *Nat. Resour. Res.*, **30** (2021), 4773–4788. https://doi.org/10.1007/S11053-021-09930-5
4. V. Balakrishnan, P. Rai, An overview of flyrock and its prediction in surface mine blasting using soft computing techniques, *Recep Tayyip Erdogan Univ. J. Sci. Eng.*, **2** (2021), 105–119. https://doi.org/10.53501/rteufemud.986903
5. R. Zhang, Y. Li, Y. Gui, J. Zhou, Prediction of blasting induced air-overpressure using a radial basis function network with an additional hidden layer, *Appl. Soft Comput.*, **127** (2022), 109343. https://doi.org/10.1016/j.asoc.2022.109343

6. S. Hosseini, R. Poormirzaee, M. Hajihassani, Application of reliability-based back-propagation causality-weighted neural networks to estimate air-overpressure due to mine blasting, *Eng. Appl. Artif. Intell.*, **115** (2022), 105281. https://doi.org/10.1016/j.engappai.2022.105281
7. R. Shirani Faradonbeh, D. Jahed Armaghani, M. Abd Majid, M. Md Tahir, B. Ramesh Murlidhar, M. Monjezi, et al., Prediction of ground vibration due to quarry blasting based on gene expression programming: a new model for peak particle velocity prediction, *Int. J. Environ. Sci. Technol.*, **13** (2016), 1453–1464. https://doi.org/10.1007/s13762-016-0979-2
8. E. Bakhtavar, S. Yousefi, Analysis of ground vibration risk on mine infrastructures: Integrating fuzzy slack-based measure model and failure effects analysis, *Int. J. Environ. Sci. Technol.*, **16** (2019), 6065–6076. https://doi.org/10.1007/s13762-018-2008-0
9. V. N. Torres, L. G. Silveira, P. F. Lopes, H. M. De Lima, Assessing and controlling of bench blasting-induced vibrations to minimize impacts to a neighboring community, *J. Clean. Prod.*, **187** (2018), 514–524. https://doi.org/10.1016/j.jclepro.2018.03.210
10. K. Peng, J. Zeng, D. J. Armaghani, M. Hasanipanah, Q. Chen, A novel combination of gradient boosted tree and optimized ANN models for forecasting ground vibration due to quarry blasting, *Nat. Resour. Res.*, **30** (2021), 4657–4671. https://doi.org/10.1007/s11053-021-09899-1
11. A. I. Lawal, S. Kwon, G. Y. Kim, Prediction of the blast-induced ground vibration in tunnel blasting using ANN, moth-flame optimized ANN, and gene expression programming, *Acta Geophys.*, **69** (2021), 161–174. https://doi.org/10.1007/s11600-020-00532-y
12. R. S. Faradonbeh, M. Monjezi, Prediction and minimization of blast-induced ground vibration using two robust meta-heuristic algorithms, *Eng. Comput.*, **33** (2017), 835–851. https://doi.org/10.1007/s00366-017-0501-6
13. A. Kumar, P. Singh, S. K. Sharma, N. Kishore, C. Singh, Quantitative assessment of BIGV and structural response based on velocity and frequency around an opencast mine, *Curr. Sci.*, **121** (2021), 275–285. https://doi.org/10.18520/cs/v121/i2/275-285
14. K. Norén-Cosgriff, N. Ramstad, A. Neby, C. Madshus, Building damage due to vibration from rock blasting, *Soil Dyn. Earthquake Eng.*, **138** (2020), 106331. https://doi.org/10.1016/j.soildyn.2020.106331
15. A. Verkholantsev, R. Dyagilev, D. Y. Shulakov, A. Shkurko, Monitoring of earthquake loads from blasting in the shakhtau open pit mine, *J. Min. Sci.*, **55** (2019), 229–238. https://doi.org/10.1134/S1062739119025503
16. M. P. Roy, A. K. Mishra, H. Agrawal, P. K. Singh, Blast vibration dependence on total explosives weight in open-pit blasting, *Arabian J. Geosci.*, **13** (2020), 531. https://doi.org/10.1007/s12517-020-05560-y
17. M. Rezaei, Modeling and optimizing the drilling and blasting pattern of the Boghde-Kandi quarry rubble mine of Saghez, *Iran. J. Eng. Geol.*, **11** (2019), 41–53.
18. A. Rezaeineshat, M. Monjezi, A. Mehrdanesh, M. Khandelwal, Optimization of blasting design in open pit limestone mines with the aim of reducing ground vibration using robust techniques, *Geomech. Geophys. Geo Energy Geo Resour.*, **6** (2020), 40. https://doi.org/10.1007/s40948-020-00164-y
19. P. Sun, W. Lu, J. Zhou, X. Huang, M. Chen, Q. Li, Comparison of dominant frequency attenuation of blasting vibration for different charge structures, *J. Rock Mech. Geotech. Eng.*, **14** (2022), 448–459. https://doi.org/10.1016/j.jrmge.2021.07.002

20. P. Paurush, P. Rai, S. K. Sharma, Selection of blasting design parameters affecting peak particle velocity—a case study, *Min. Metall. Explor.*, **38** (2021), 1435–1447. https://doi.org/10.1007/s42461-021-00408-9
21. T. Mokfi, A. Shahnazar, I. Bakhshayeshi, A. M. Derakhsh, O. Tabrizi, Proposing of a new soft computing-based model to predict peak particle velocity induced by blasting, *Eng. Comput.*, **34** (2018), 881–888. https://doi.org/10.1007/s00366-018-0578-6
22. Y. S. Chae, Effects of blasting vibrations on structures and people, In: *Proceedings of 19th US symposium on rock mechanics*, 1978, 312–318.
23. J. Zhou, W. Lu, P. Yan, M. Chen, G. Wang, Frequency-dependent attenuation of blasting vibration waves, *Rock Mech. Rock Eng.*, **49** (2016), 4061–4072. https://doi.org/10.1007/s00603-016-1046-5
24. M. Khandelwal, T. Singh, Prediction of blast induced ground vibrations and frequency in opencast mine: A neural network approach, *J. Sound Vib.*, **289** (2006), 711–725. https://doi.org/10.1016/j.jsv.2005.02.044
25. C. H. Dowding, Blast vibration monitoring for engineering, *Excav. Support Monit.*, **4** (2016), 111.
26. E. F. Gad, J. L. Wilson, A. J. Moore, A. B. Richards, Effects of mine blasting on residential structures, *J. Perform. Constr. Facil.*, **19** (2005), 222–228. https://doi.org/10.1061/(ASCE)0887-3828(2005)19:3(222)
27. E. K. Baliktsis, D. C. Kaliampakos, D. G. Damigos, Blasting vibration limits to prevent human annoyance remarks from some case studies, *Miner. Resour. Eng.*, **10** (2001), 71–82. https://doi.org/10.1142/S0950609801000452
28. C. P. Singh, H. Agrawal, A. K. Mishra, Frequency channeling: a concept to increase the frequency and control the PPV of blast-induced ground vibration waves in multi-hole blast in a surface mine, *Bull. Eng. Geol. Environ.*, **80** (2021), 8009–8019. https://doi.org/10.1007/s10064-021-02400-5
29. P. Rajmeny, R. Shrimali, Use of radar technology to establish threshold values of blast vibrations triggering sliding of geological faults at a lead-zinc open pit mine, *Int. J. Rock Mech. Min. Sci.*, **113** (2019), 142–149. https://doi.org/10.1016/j.ijrmms.2018.12.004
30. S. Zhang, W. Gao, L. Yan, J. Liu, L. Liu, The characteristics of blasting vibration frequency bands in jointed rock mass slope, *Environ. Earth Sci.*, **79** (2020), 519. https://doi.org/10.1007/s12665-020-09267-x
31. M. Hasanipanah, M. Monjezi, A. Shahnazar, D. J. Armaghani, A. Farazmand, Feasibility of indirect determination of blast induced ground vibration based on support vector machine, *Measurement*, **75** (2015), 289–297. https://doi.org/10.1016/j.measurement.2015.07.019
32. J. Zhou, P. G. Asteris, D. J. Armaghani, B. T. Pham, Prediction of ground vibration induced by blasting operations through the use of the Bayesian Network and random forest models, *Soil Dyn. Earthquake Eng.*, **139** (2020), 106390. https://doi.org/10.1016/j.soildyn.2020.106390
33. S. Murmu, P. Maheshwari, H. K. Verma, Empirical and probabilistic analysis of blast-induced ground vibrations, *Int. J. Rock Mech. Min. Sci.*, **103** (2018), 267–274. https://doi.org/10.1016/j.ijrmms.2018.01.038
34. A. Abolghasemifar, M. Ataei, S. R. Torabi, M. Nikkhah, Studying peak particle velocity due to blast in development tunnels' face in coal stoping, *Int. J. Min. Geo Eng.*, **52** (2018), 69–74. https://doi.org/10.22059/ijmge.2017.241867.594698

35. A. Das, S. Sinha, S. Ganguly, Development of a blast-induced vibration prediction model using an artificial neural network, *J. South. Afr. Inst. Min. Metall.*, **119** (2019), 187–200. https://doi.org/10.17159/2411-9717/2019/v119n2a11
36. N. Torres, J. A. Reis, P. L. Luiz, J. H. R. Costa, L. S. Chaves, Neural network applied to blasting vibration control near communities in a large-scale iron ore mine, In: *Proceedings of the 27th international symposium on mine planning and equipment selection-MPES 2018*, Cham: Springer, 2019, 81–91. https://doi.org/10.1007/978-3-319-99220-4_7
37. A. Bardhan, P. G. Asteris, Application of hybrid ANN paradigms built with nature inspired meta-heuristics for modelling soil compaction parameters, *Transp. Geotech.*, **41** (2023), 100995. https://doi.org/10.1016/j.trgeo.2023.100995
38. W. Zhu, H. N. Rad, M. Hasanipanah, A chaos recurrent ANFIS optimized by PSO to predict ground vibration generated in rock blasting, *Appl. Soft Comput.*, **108** (2021), 107434. https://doi.org/10.1016/j.asoc.2021.107434
39. A. Meng, Z. Zhu, W. Deng, Z. Ou, S. Lin, C. Wang, et al., A novel wind power prediction approach using multivariate variational mode decomposition and multi-objective crisscross optimization based deep extreme learning machine, *Energy*, **260** (2022), 124957. https://doi.org/10.1016/j.energy.2022.124957
40. H. Yang, Y. Cheng, G. Li, A new traffic flow prediction model based on cosine similarity variational mode decomposition, extreme learning machine and iterative error compensation strategy, *Eng. Appl. Artif. Intell.*, **115** (2022), 105234. https://doi.org/10.1016/j.engappai.2022.105234
41. Y. Wang, D. Li, Y. Du, Z. Pan, Anomaly detection in traffic using L1-norm minimization extreme learning machine, *Neurocomputing*, **149** (2015), 415–425. https://doi.org/10.1016/j.neucom.2014.04.073
42. D. Reshef, Y. Reshef, M. Mitzenmacher, P. Sabeti, Equitability analysis of the maximal information coefficient, with comparisons, *arXiv*, 2013. https://doi.org/10.48550/arXiv.1301.6314
43. J. Xue, B. Shen, Dung beetle optimizer: a new meta-heuristic algorithm for global optimization, *J. Supercomput.*, **79** (2023), 7305–7336. https://doi.org/10.1007/s11227-022-04959-6
44. S. Mirjalili, A. Lewis, The whale optimization algorithm, *Adv. Eng. Software*, **95** (2016), 51–67. https://doi.org/10.1016/j.advengsoft.2016.01.008
45. S. Mirjalili, S. M. Mirjalili, A. Lewis, Grey wolf optimizer, *Adv. Eng. Software*, **69** (2014), 46–61. https://doi.org/10.1016/j.advengsoft.2013.12.007
46. M. Dehghani, Š. Hubálovský, P. Trojovský, Northern goshawk optimization: a new swarm-based algorithm for solving optimization problems, *IEEE Access*, **9** (2021), 162059–162080. https://doi.org/10.1109/ACCESS.2021.3133286
47. A. A. Heidari, S. Mirjalili, H. Faris, I. Aljarah, M. Mafarja, H. Chen, Harris hawks optimization: algorithm and applications, *Future Gener. Comput. Syst.*, **97** (2019), 849–872. https://doi.org/10.1016/j.future.2019.02.028
48. H. Nguyen, X. N. Bui, E. Topal, Enhancing predictions of blast-induced ground vibration in open-pit mines: comparing swarm-based optimization algorithms to optimize self-organizing neural networks, *Int. J. Coal Geol.*, **275** (2023), 104294. https://doi.org/10.1016/j.coal.2023.104294

49. H. Nguyen, X. N. Bui, E. Topal, Reliability and availability artificial intelligence models for predicting blast-induced ground vibration intensity in open-pit mines to ensure the safety of the surroundings, *Reliab. Eng. Syst. Saf.*, **231** (2023), 109032. https://doi.org/10.1016/j.ress.2022.109032
50. H. Nguyen, X. N. Bui, Q. H. Tran, H. A. Nguyen, D. A. Nguyen, L. T. T. Hoa, et al., Prediction of ground vibration intensity in mine blasting using the novel hybrid MARS-PSO-MLP model, *Eng. Comput.*, **38** (2022), 4007–4025. https://doi.org/10.1007/s00366-021-01332-8
51. B. Ke, H. Nguyen, X. N. Bui, R. Costache, Estimation of ground vibration intensity induced by mine blasting using a state-of-the-art hybrid autoencoder neural network and support vector regression model, *Nat. Resour. Res.*, **30** (2021), 3853–3864. https://doi.org/10.1007/s11053-021-09890-w
52. H. Nguyen, X. N. Bui, A novel hunger games search optimization-based artificial neural network for predicting ground vibration intensity induced by mine blasting, *Nat. Resour. Res.*, **30** (2021), 3865–3880. https://doi.org/10.1007/s11053-021-09903-8
53. Z. Yu, X. Shi, J. Zhou, X. Chen, X. Qiu, Effective assessment of blast-induced ground vibration using an optimized random forest model based on a Harris hawks optimization algorithm, *Appl. Sci.*, **10** (2020), 1403. https://doi.org/10.3390/app10041403
54. H. Nguyen, X. N. Bui, H. B. Bui, D. T. Cuong, Developing an XGBoost model to predict blast-induced peak particle velocity in an open-pit mine: A case study, *Acta Geophys.*, **67** (2019), 477–490. https://doi.org/10.1007/s11600-019-00268-4

AIMS Press